

# X-ray diffraction peak profiles from threading dislocations in GaN epitaxial films

V. M. Kaganer, O. Brandt, A. Trampert, and K. H. Ploog

*Paul-Drude-Institut für Festkörperelektronik, Hausvogteiplatz 5-7, D-10117 Berlin, Germany*

(Dated: November 26, 2024)

We analyze the lineshape of x-ray diffraction profiles of GaN epitaxial layers with large densities of randomly distributed threading dislocations. The peaks are Gaussian only in the central, most intense part of the peak, while the tails obey a power law. The  $q^{-3}$  decay typical for random dislocations is observed in double-crystal rocking curves. The entire profile is well fitted by a restricted random dislocation distribution. The densities of both edge and screw threading dislocations and the ranges of dislocation correlations are obtained.

## I. INTRODUCTION

GaN epitaxial layers grown on different substrates (e.g.,  $\text{Al}_2\text{O}_3$ , SiC, or Si) possess very large densities of threading dislocations which cross the layer along its normal, from the layer-substrate interface to the surface.<sup>1</sup> The threading dislocation density depends only marginally on the substrate material (and hence on the misfit between the substrate and the layer) but rather on the growth technique and conditions. For (0001) oriented layers of wurtzite GaN, the overwhelming majority of dislocations are of edge type with Burgers vectors  $\mathbf{b} = \frac{1}{3}\langle 11\bar{2}0 \rangle$ . Their density<sup>2,3,4,5,6</sup> is typically  $10^8 - 10^{10} \text{ cm}^{-2}$ . The density of screw dislocations with Burgers vector  $\mathbf{b} = [0001]$  is one to two orders of magnitude lower than the density of edge dislocations.

The dislocation density can be measured directly by plan-view transmission electron microscopy (TEM). The actual virtue of TEM is not the accurate determination of the dislocation density, but rather the possibility to determine the type of the dislocation distribution (e. g., random vs. granular/columnar structure). It is of limited statistical significance considering the small area covered by TEM micrographs. Alternatively, x-ray diffraction can be used to detect the lattice distortions due to the presence of dislocations. In principle, both the disloca-

tion distribution and the actual dislocation density may be obtained from x-ray diffraction profiles.

The impact of screw and edge threading dislocations on the width of the x-ray reflections in the limiting cases of lattice planes parallel and perpendicular to the surface is commonly referred to as tilt and twist, respectively.<sup>2,3,4,5,6</sup> This designation stems from the model of misoriented blocks<sup>6</sup> which is *not* appropriate for strains caused by randomly distributed dislocations. In this case, the description in terms of mean-squared distortions<sup>7</sup> is actually more adequate. Moreover, all previous experimental studies only use the full width at half-maximum (FWHM) of different reflections as a measure of the dislocation density.

The symmetric Bragg reflections from GaN layers are comparatively narrow, since they are not influenced by the presence of edge dislocations. Edge dislocations produce distortions within lattice planes parallel to the surface but do not disturb positions of these planes along the layer normal. The highest sensitivity to edge dislocations is obtained by diffraction from lattice planes perpendicular to the surface. This diffraction geometry requires grazing incidence illumination and is thus commonly performed at a synchrotron.<sup>8,9</sup> An alternative geometry that can easily be realized in the laboratory is the skew geometry,<sup>2,5</sup> which is a quasi-symmetric (the incident and the diffracted waves have the same angles to the surface) non-coplanar (the surface normal does not lie in the plane defined by the incident and the diffracted waves) geometry, as shown in Fig. 1. By measuring different reflections with increasing lattice plane inclination, one can extrapolate to lattice planes perpendicular to the surface.<sup>2,5</sup> A single reflection with a large inclination can be regarded as a figure of merit.<sup>4</sup> A four-circle diffractometer<sup>10</sup> is required for skew geometry measurements, since the sample has to be tilted with respect to its surface normal. Coplanar asymmetric reflections on a three-circle diffractometer are much less sensitive to edge dislocations since they only partially touch the lattice distortions parallel to the surface plane.<sup>5</sup>

The FWHM of the diffraction peak depends not only on the dislocation density, but also on the correlations between dislocations. Furthermore, it depends on the mutual orientations of the scattering vector, dislocation line direction, and the Burgers vector direction, which have not been taken into consideration in previous diffraction

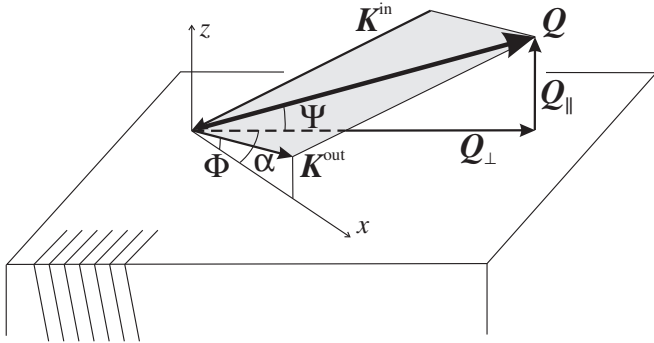


FIG. 1: Sketch of skew geometry x-ray diffraction. The lattice planes of the actual reflection are depicted in the left bottom part of the figure. The incident wave  $\mathbf{K}^{\text{in}}$  and the diffracted wave  $\mathbf{K}^{\text{out}}$  make the same angle  $\Phi$  to the sample surface. The scattering vector  $\mathbf{Q}$  makes an angle  $\Psi$  to the sample surface.

studies of GaN layers. In the present paper, we analyze the entire lineshape of the diffraction profiles, and particularly their tails. These tails are due to scattering in the close vicinity of the dislocation lines and are not influenced by the correlations between dislocations. They follow universal power laws and can be used to determine the dislocation density. We fit the entire diffraction peak profile to the numerical Fourier transform of the pair correlation function and simultaneously obtain dislocation densities and the range of dislocation correlations.

## II. BACKGROUND

X-ray diffraction is a well-established technique to analyze crystal lattice imperfections.<sup>11,12</sup> The conventional and widely used methods (also in GaN studies<sup>6</sup>) are based on a comparison of the diffraction peak widths of different reflections.<sup>13,14,15</sup> They aim to separate two contributions to the peak broadening, the finite size of the crystalline domains (grains) in the sample and the non-uniform strain within each domain owing to lattice defects. The strain broadening of a diffraction peak is proportional to the length of the scattering vector, while the size effect does not depend on it. Thus, comparing the peak widths of reflections of successive orders in the so-called Williamson-Hall plot, one can separate both contributions. The separation method assumes that all peaks are Gaussian,<sup>14,15</sup> or all Lorentzian.<sup>13</sup> This is certainly not true, and the methods based on the peak width give only rough, albeit instructive, estimates of the crystal perfection. A recent development<sup>16,17,18</sup> includes corrections for given orientations of the dislocation lines and Burgers vectors with respect to the scattering vector.

The next milestone was the Fourier analysis of the diffraction peak profile proposed by Warren and Averbach.<sup>19,20</sup> The starting point of their analysis is the average over grain orientations in powder diffraction. The corresponding integration of the scattered intensity in reciprocal space is equivalent to a one-dimensional cut of the correlation function in real space. We note that the powder diffraction literature does not use the term correlation function but refers to the Fourier coefficients of the intensity. We use the solid-state physics terminology where this quantity is commonly called the pair correlation function. In crystallography, the same function is referred to as Patterson function.

The Ansatz of the Warren-Averbach analysis is the assumption that the correlation function is a product of two independent terms describing the size and the strain effects, respectively. Furthermore, it is assumed that the finite sizes of the grains give rise to a Lorentzian peak (exponential correlation function) while non-uniform strain is described by a Gaussian function. With these assumptions, the size and strain effects are separated by differentiation of the Fourier-transformed peak profile. In many cases, the latter step is not sufficiently accurate, since it has to rely on a few Fourier coefficients obtained

from noisy experimental data. Balzar<sup>21,22</sup> suggested to avoid this difficulty by directly fitting the peak profile to a convolution of a Lorentzian and a Gaussian, which is the Voigt function. The experimental peak profiles are not always described by the Voigt function and various other analytical functions were suggested on a purely phenomenological basis.<sup>23,24</sup>

The assumption that non-uniform strain gives rise to a Gaussian correlation function looks plausible, taking into account the stochastic nature of this strain originating from randomly distributed lattice defects. However, Krivoglaz and Ryboshapka<sup>12,25</sup> have shown that this is not true for random dislocations, which are the most common and most important source of strain. Rather, they found that the slow ( $\propto r^{-1}$ ) decay of the strain with the distance  $r$  from the dislocation line gives rise to a correlation function

$$G(x) = \exp(-C\rho x^2 \ln \frac{L}{\xi x}). \quad (1)$$

Here  $C \sim 1$  is a dimensionless factor depending on the orientations of the dislocation line and Burgers vector with respect to the  $x$ -direction (an arbitrary direction along which the correlations are measured). Its dependence on the scattering vector  $\mathbf{Q}$  and the Burgers vector  $\mathbf{b}$  is given by  $C \propto (\mathbf{Q} \cdot \mathbf{b})^2$ . The dislocation density  $\rho$  is defined as a total length of the dislocation lines per unit volume. For straight dislocations,  $\rho$  is equal to the number of dislocations crossing the unit area of a plane perpendicular to the dislocation lines.  $\xi \sim 1$  is another dimensionless factor, for uncorrelated dislocations  $\xi = |\mathbf{Q} \cdot \mathbf{b}|/2\pi$ .

For completely random and uncorrelated dislocations,  $L$  is the crystal size, so that the diffraction peak width of an infinite crystal with random uncorrelated dislocations tends to infinity. Wilkens<sup>26,27,28</sup> pointed out that this divergence has the same origin as the divergence of elastic energy of a crystal with dislocations: the elastic energy is proportional to  $\mu b^2 \ln L/a$ , where  $\mu$  is the shear modulus,  $b$  is the length of the Burgers vector, and  $a$  is the lattice spacing. He suggested that the system can drastically reduce elastic energy by a very minor rearrangement in the dislocation ensemble: the positions of the dislocations remain random but their Burgers vectors are correlated, so that the total Burgers vector in a region exceeding some characteristic scale is zero. Then, the dislocations screen each other and the elastic energy, as well as the diffraction peak width, remain finite. Wilkens introduced a “restricted random distribution” of dislocations by subdividing the crystal into cells, such that the total Burgers vector in each cell is zero. He found<sup>26,27,28</sup> that the functional form of Eq. (1) does not change but  $L$  should be understood as a finite size of the cells. Krivoglaz *et al.*<sup>12,29</sup> showed that the same result is valid for a broad class of correlated dislocation distributions with screening.

We note also the two-dimensional crystal as a limiting case of dislocation screening. Here the elastic en-

ergy of dislocations is to be compared with the entropic term  $-TS$ , where  $T$  is temperature and the entropy  $S = \ln(L/a)^2$  is the number of lattice sites where the dislocation can be placed. Both elastic energy and entropy terms are proportional to  $\ln L$ . As a result, above some temperature  $T_m$ , dislocations are generated by unbinding of thermally excited dislocation pairs, giving rise to the dislocation mediated melting.<sup>30,31</sup> The calculation of the correlation function in this highly correlated dislocation system<sup>32</sup> shows that the logarithmic term in Eq. (1) vanishes.

Fourier transformation of the correlation function (1) yields a Gaussian shape only in the central part of the peak. The range of the Gaussian peak shape is given by a dimensionless factor

$$M = L\sqrt{\rho} \quad (2)$$

and increases when  $M$  is increased. The intensity distribution notably deviates from the Gaussian shape at the tails of the diffraction peak.

The tails of the diffraction peak due to dislocations follow a universal law  $I(q) \propto q^{-3}$ , which can be obtained from Fourier transformation of Eq. (1).<sup>33</sup> The  $q^{-3}$  law is due to the fact that at large  $q$ , the scattering takes place in the strained regions close to dislocation lines, where the lattice is so strongly misoriented that the Bragg law is locally satisfied for the wave vector  $q$ . Calculation of the volume of these regions give the  $q^{-3}$  dependence.<sup>12,33,34</sup> Groma and co-workers<sup>33,35,36</sup> developed methods for the peak profile analysis based on a calculation of the restricted moments of  $I(q)$ . In particular, the second-order restricted moment  $v(q) = \int_{-q}^q q^2 I(q) dq$  is proportional to  $\ln q$ , which they used to determine the mean dislocation density. Higher-order moments describe fluctuations of the dislocation density.

GaN epitaxial film comprise a well-defined system where threading dislocations are aligned perpendicular to the surface plane. The film is oriented, contrary to a powder. However, the x-ray diffraction measurements performed with an open detector give rise to an average very similar to the powder average. The intensity is integrated over directions of the outgoing beam, instead of the integration over directions of the diffraction vector. The integrations in reciprocal space gives rise to cuts in real space, which are different for the two cases under consideration. The coordinate  $x$  in Eq. (1) runs along the direction of the outgoing wave in case of the oriented sample with open detector and in the direction of the diffraction vector for the case of powder diffraction. This fact introduces a geometrical correction in the orientational factor  $C$ . The skew diffraction geometry used for the measurements gives rise to further corrections, which are calculated below.

Our approach consists of a direct fit of the measured intensities by the numerical Fourier transformation of the correlation function (1), thus avoiding any transformation of the experimental data. We expect that such a calculation is less influenced by the noise in the experi-

mental data and is more reliable. As shown below, we find good agreement between measured and calculated peak profiles. From the fits, we reliably obtain both the dislocation densities and the correlation range in the restricted random dislocation distribution.

### III. THEORY

The intensity of x-ray scattering from a crystal disturbed by strain fields of lattice defects can be represented as a Fourier transform

$$I(\mathbf{q}) = \int G(\mathbf{r}) \exp(i\mathbf{q} \cdot \mathbf{r}) d\mathbf{r} \quad (3)$$

of the pair correlation function

$$G(\mathbf{r}) = \langle \exp\{i\mathbf{Q} \cdot [\mathbf{U}(\mathbf{r}) - \mathbf{U}(0)]\} \rangle. \quad (4)$$

Here  $\mathbf{Q} = \mathbf{K}^{\text{out}} - \mathbf{K}^{\text{in}}$  is the scattering vector ( $\mathbf{K}^{\text{in}}$  and  $\mathbf{K}^{\text{out}}$  are the wave vectors of the incident and scattered waves, respectively) and  $\mathbf{q} = \mathbf{Q} - \mathbf{Q}_0$  is a small deviation of  $\mathbf{Q}$  from the nearest reciprocal lattice vector  $\mathbf{Q}_0$ , so that  $q \ll Q$ .  $\mathbf{U}(\mathbf{r})$  is the sum of displacements produced by all defects of the crystal in a given point  $\mathbf{r}$  and  $\langle \dots \rangle$  denotes the average over the statistics of the defect distribution. Equation (4) implies an infinite and statistically uniform sample, so that the choice of origin is arbitrary. When finite size effects are essential, as for example for misfit dislocations in epitaxial layers,<sup>37</sup> the correlation function  $G(\mathbf{r}_1, \mathbf{r}_2)$  depends on the difference of displacements  $\mathbf{U}(\mathbf{r}_1) - \mathbf{U}(\mathbf{r}_2)$  and Eq. (3) contains the exponent  $\exp[i\mathbf{q} \cdot (\mathbf{r}_1 - \mathbf{r}_2)]$ .

We restrict ourselves to parallel straight dislocations and take the direction of the dislocation lines as  $z$  axis. Then,  $\mathbf{r} = (x, y)$  is a two-dimensional vector in the plane perpendicular to the dislocation lines and Eq. (3) can be written as

$$I(\mathbf{q}) = \delta(q_z) \int G(x, y) \exp(iq_x x + iq_y y) dx dy, \quad (5)$$

where the delta-function  $\delta(q_z)$  is due to the translational invariance in the direction of the dislocation lines.

In the experiments described in the subsequent sections, the x-ray scattering measurements from oriented samples are performed with a wide open detector. The intensity (3) is then to be integrated over all directions of the scattered wave  $\mathbf{K}^{\text{out}}$ . The result of this integration is very similar to the powder average. The actual part of the sphere  $|\mathbf{K}^{\text{out}}| = k$  (where  $k$  is the wave vector) can be replaced by the plane perpendicular to the direction of  $\mathbf{K}^{\text{out}}$ . Integration of the intensity (5) over this plane gives rise to a one-dimensional integral

$$\mathcal{I}(q) = \int G(x) \exp(iqx / \cos \Phi) dx, \quad (6)$$

where  $\Phi$  is the angle between the  $(x, y)$  plane and  $\mathbf{K}^{\text{out}}$  (see Fig. 1). It is given by  $\sin \Phi = \sin \Psi \sin \theta_B$ , where  $\Psi$

is the angle between the  $(x, y)$  plane and the scattering vector  $\mathbf{Q}$  and  $\theta_B$  is the Bragg angle. The  $x$  axis is chosen along the projection of  $\mathbf{K}^{\text{out}}$  on the plane perpendicular to the dislocation lines. The corresponding expression for the case of powder diffraction differs only by the direction of  $x$ : it runs along  $\mathbf{K}^{\text{out}}$  for oriented films and along  $\mathbf{Q}$  for powder diffraction. The wave vector  $q$  in Eq. (6) is the projection of  $\mathbf{q}$  on the direction of  $\mathbf{K}^{\text{out}}$ , so that  $q = Q\omega \cos \theta_B$ , where  $\omega$  is the angular deviation from the peak center.

Krivoglaz<sup>12,25,38</sup> performed the average over an uncorrelated defect distribution and showed that the correlation function can be represented as

$$G(\mathbf{r}) = \exp \left\{ -\rho \int \left[ 1 - e^{i\mathbf{Q} \cdot [\mathbf{u}(\mathbf{R}+\mathbf{r}) - \mathbf{u}(\mathbf{R})]} \right] d\mathbf{R} \right\}. \quad (7)$$

Here  $\mathbf{u}(\mathbf{r})$  is the displacement field produced at a point  $\mathbf{r}$  by a single defect located at the origin and  $\rho$  is the defect density. For straight dislocations, the integration in Eq. (7) is performed over the  $\mathbf{R} = (X, Y)$  plane perpendicular to the dislocation lines and  $\rho$  is the dislocation density per unit area. Thus, according to Eq. (7), in order to obtain positional correlations between two points separated by a distance  $\mathbf{r}$ , one has to place a dislocation in an arbitrary position  $\mathbf{R}$  and perform the integration over all  $\mathbf{R}$ .

As a result of the slow decay of the dislocation strain, the main contribution to the integral is due to remote dislocations,  $R \gg r$ , so that the difference of displacements can be expanded as Taylor series,  $\mathbf{Q} \cdot [\mathbf{u}(\mathbf{R} + \mathbf{r}) - \mathbf{u}(\mathbf{R})] \approx (\mathbf{r} \cdot \nabla)[\mathbf{Q} \cdot \mathbf{u}(\mathbf{R})] = r_i Q_j \partial u_j / \partial X_i$ . The distortion field of a dislocation has a universal  $r$ -dependence,  $\partial u_j / \partial X_i = b\psi_{ij} / 2\pi R$ , where  $b$  is the length of the Burgers vector and  $\psi_{ij}$  is a dimensionless factor of the order of unity which depends only on the azimuth  $\phi$ . If the densities of dislocations with opposite signs of the Burgers vectors are equal (there is no plastic bend), the imaginary part of the correlation function (7) is zero and its real part, after expanding the exponent in curly brackets, becomes<sup>25</sup>

$$G(\mathbf{r}) = \exp \left\{ -C\rho r^2 \int \frac{dR}{R} \right\}, \quad (8)$$

where

$$C = \gamma(Qb)^2 / 4\pi, \quad \gamma = \frac{1}{2\pi} \int_0^{2\pi} \left( \hat{r}_i \psi_{ij} \hat{Q}_j \right)^2 d\phi. \quad (9)$$

$C$  and  $\gamma$  are dimensionless factors of the order of unity. Here  $\hat{\mathbf{r}}$  and  $\hat{\mathbf{Q}}$  are unit vectors in the directions of  $\mathbf{r}$  and  $\mathbf{Q}$ , respectively. The integral in Eq. (8) is taken from  $\xi r$  (where  $\xi \sim 1$  is a dimensionless factor) to a limiting size  $L$ , which, for completely uncorrelated dislocations, is equal to the crystal size. Then, the integral is equal to  $\ln(L/\xi r)$ , and we arrive at Eq. (1). When the dislocations are correlated, so that the total Burgers vector averaged over a certain characteristic scale is zero, the functional form of the correlation function does not change but  $L$  has the meaning of that scale.<sup>12,26,27,28,29</sup>

The integration range in Eq. (6) is limited by distances smaller than  $L$ . A finite integration limit introduced in Eq. (6) leads, in a numerical evaluation of the integral, to unphysical oscillations in  $\mathcal{I}(q)$  commonly appearing in Fourier integrals taken over a rigidly limited interval. We found that an appropriate smoothing is obtained by substituting  $\ln(L/\xi x)$  in Eq. (1) with  $\ln[(L + \xi x)/\xi x]$  and extending the integration range to infinity. The expressions for  $\xi = \xi(\mathbf{Q})$  are bulky and depend on the type of correlations in dislocation positions.<sup>12,27,28,29</sup> We restrict ourselves to the first approximation that does not depend on the type of correlations,  $\xi = |\mathbf{Q} \cdot \mathbf{b}| / 2\pi$ .

Finally, combining the equations above, the diffracted intensity can be represented as

$$\mathcal{I}(\omega) = I_0 \int_0^\infty \exp(-Ax^2 \ln \frac{B+x}{x}) \cos(\omega x) dx + I_{\text{backgr}}. \quad (10)$$

We proceed here to the angular deviation from the peak maximum  $\omega$  and introduce the peak height  $I_0$  and the background intensity  $I_{\text{backgr}}$  to provide the exact formula that is used for the fits of the experimental peaks presented below. Parameters  $A$  (describing the dislocation density) and  $B$  (describing the dislocation correlation range) are given by

$$A = f\rho b^2, \quad B = gL/b. \quad (11)$$

Here  $f$  and  $g$  are dimensionless quantities given by the diffraction geometry,

$$f = \frac{\gamma}{4\pi} \frac{\cos^2 \Phi}{\cos^2 \theta_B}, \quad g = \frac{2\pi \cos \theta_B}{\cos \Phi \cos \Psi}. \quad (12)$$

In Eq. (12), the expression for  $g$  is written for edge dislocations, taking into account the approximation  $\xi = |\mathbf{Q} \cdot \mathbf{b}| / 2\pi$ . For screw dislocations,  $\cos \Psi$  in this expression should be replaced by  $\sin \Psi$ . The length of the Burgers vector  $b$  in Eq. (11) is that of the relevant Burgers vector for either edge or screw dislocations. The dimensionless product  $\rho b^2 \ll 1$  is the mean number of dislocations crossing each  $b \times b$  cell in the plane perpendicular to the dislocation lines. Equation (10) with four parameters,  $A, B, I_0, I_{\text{backgr}}$  is used in Sec. V below to fit the peak profiles and obtain the dislocation density  $\rho$  and the length  $L$ .

The behavior of the integral (10) is illustrated in Fig. 2 where the function

$$I(q) = \int_0^\infty \exp\{-x^2 \ln[(R+x)/x]\} \cos(qx) dx \quad (13)$$

is numerically calculated for different values of the parameter  $R$ . The curves merge at a common  $q^{-3}$  asymptotic that does not depend on  $R$ .<sup>12,28,33,35</sup> Then, Eq. (10) has an asymptotic behavior (for  $\omega$  large in comparison with the peak width)

$$\mathcal{I}(\omega) = A \frac{\pi I_0}{\omega^3} + I_{\text{backgr}}. \quad (14)$$

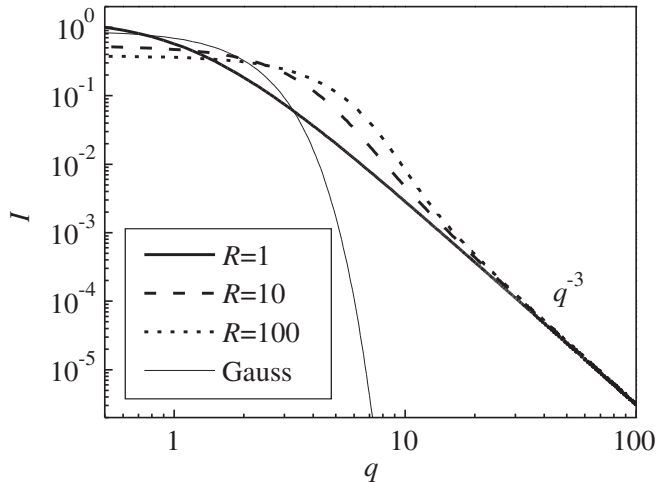


FIG. 2: Behavior of the integral (13) for different values of the parameter  $R$ . All curves merge at a common  $q^{-3}$  asymptotic. A Gaussian peak profile is shown by the thin line for comparison.

We note that  $\pi I_0$  is the integrated intensity of the peak.

Figure 2 also shows that the asymptotics (14) is reached quite close to the peak center for  $R \sim 1$ , while for  $R \gg 1$  the central part of the peak is Gaussian and the angular range where the Gaussian approximation is valid increases with increasing  $R$ . The FWHM of the calculated peaks increases with increasing  $R$  and can be approximated by

$$\Delta q \approx 2.4 + \ln R. \quad (15)$$

Groma<sup>33</sup> suggested to use the second restricted moment of the intensity distribution

$$v_2(\omega) = \int_{-\omega}^{\omega} \varpi^2 [\mathcal{I}(\varpi) - I_{\text{backgr}}] d\varpi \quad (16)$$

to obtain the dislocation density from the asymptotic behavior (14). Note that the integral (16) diverges, when taken in infinite limits. One finds, by substituting (14) into (16), that

$$v_2(\omega) = 2\pi I_0 A \ln \omega + \text{const.} \quad (17)$$

It remains to calculate the orientational factor  $C$  [Eq. (9)]. In the case of powder diffraction,<sup>26,27,28</sup> the vector  $\mathbf{r}$  is directed along the projection  $\mathbf{Q}_{\perp}$  of the scattering vector  $\mathbf{Q}$  on the  $(x, y)$  plane. In our case, the vector  $\mathbf{r}$  is directed along the projection of  $\mathbf{K}^{\text{out}}$  on the  $(x, y)$  plane and makes an angle  $\alpha$  with the vector  $\mathbf{Q}_{\perp}$ , see Fig. 1. This angle is given by  $\cos \alpha = \sin \theta_B \cos \Psi / \cos \Phi$ . When evaluating the integral (9) for edge dislocations, we average  $\gamma$  over possible orientations of the Burgers vector in a hexagonal lattice (the dislocation lines are taken along the sixfold axis) and obtain

$$\gamma_e = \frac{9 - 8\nu + 8\nu^2 - 2(3 - 4\nu) \cos^2 \alpha}{16(1 - \nu)^2} \cos^2 \Psi, \quad (18)$$

where  $\nu$  is the Poisson ratio.  $\gamma_e$  depends only weakly on  $\alpha$ . Taking  $\nu = 1/3$ , one can approximate  $\gamma_e \approx \cos^2 \Psi$  in the whole range of reasonable angles  $\alpha$ . The calculation for screw dislocations gives

$$\gamma_s = \frac{1}{2} \sin^2 \Psi. \quad (19)$$

Two limiting cases are of interest: a symmetric Bragg reflection to study screw dislocations and a grazing incidence/grazing exit reflection as an extreme case of a highly asymmetric skew geometry. For a symmetric Bragg reflection,  $\Psi = \pi/2$  and  $\Phi = \theta_B$ . Then, we obtain  $f = 1/8\pi$  and, for screw dislocations,  $g = 2\pi$ . The grazing incidence/grazing exit geometry is the limit  $\Phi = \Psi = 0$ , so that  $f = \gamma/(4\pi \cos^2 \theta_B)$  and, for edge dislocations,  $g = 2\pi \cos \theta_B$ .

The finite thickness  $T$  of the epitaxial layer (with threading dislocations perpendicular to the layer plane) can be taken into account by making the Warren-Averbach ansatz<sup>19</sup>

$$G(x) = G_d(x)G_s(x), \quad (20)$$

where  $G_d(x)$  is the correlation function considered above. The correlation function describing finite size effects can be written as  $G_s(x) = \exp(-x/T)$ . Its Fourier transformation is a Lorentzian that is expected from the finite slit function  $[\sin(qT/2)/(qT/2)]^2$  after averaging over thickness variations. We note that, in asymmetric reflections, Eq. (6) gives rise to the effective thickness  $T/\cos \Phi$  along the direction of the diffracted wave. The finite size correction (20) does not complicate the calculation of the intensity by numerical integration of Eq. (6). If the resolution of the experiment cannot be neglected in comparison with the peak width, the correlation function (20) is to be multiplied with the real-space resolution function  $\mathcal{R}(x)$ , which also does not lead to additional complications of the numerical integration.

#### IV. EXPERIMENT

The GaN layers investigated here were grown on 6H-SiC(0001) by plasma-assisted molecular beam epitaxy (PAMBE). The two PAMBE systems employed are equipped with a solid-source effusion cell for Ga and a radio-frequency nitrogen plasma source for producing active N. Both systems have a base pressure of  $5 \times 10^{-11}$  Torr. We use 6N N<sub>2</sub> gas as a precursor which is further purified to 5 ppb by a getter filter. H<sub>2</sub>-etched 6H-SiC(0001) wafers produced by Cree<sup>TM</sup> were used as substrates.<sup>39</sup> An *in situ* Ga flash-off procedure was performed in order to remove residual suboxides from the SiC substrate surface prior to growth.<sup>39</sup> The temperatures were calibrated by visual observation of the melting point of Al (660°C) attached to the substrate.

Sample 1 was grown under Ga-stable conditions with a substrate temperature of 740°C. The growth rate em-

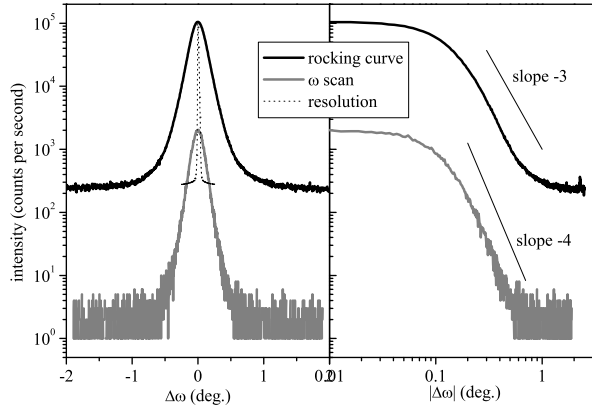


FIG. 3: Double-crystal rocking curve with open detector (black line) and triple-crystal  $\omega$  scan with analyzer (gray line) recorded in skew geometry across the 10.5 reflection of sample 1. The symmetric 004 reflection from a perfect Si crystal (broken line) is shown as a measure of the resolution. The intensities from the GaN layer are presented in counts per second, the Si(004) signal is scaled appropriately. The right panel shows the same peaks in log-log scale.

ployed was 140 nm/h, and the film was grown to a final thickness of 340 nm. Under these growth conditions, we observed an entirely streaky,  $(1 \times 1)$  RHEED pattern throughout growth except for the initial nucleation stage. The surface morphology of the film as observed by atomic force microscopy (AFM) exhibits clearly resolved monatomic steps. The root-mean-square roughness amounts to 0.3 nm over an area of  $1 \times 1 \mu\text{m}^2$ . Samples grown under these conditions typically exhibit a narrow symmetric reflection, suggesting a low density of screw dislocations. In contrast, sample 2 was grown under near-stoichiometric conditions with a substrate temperature of 780°C. The growth rate employed was 445 nm/h and the total thickness of the film amounts to 1660 nm. After the initial 100 nm of GaN growth, a 10 nm thick AlN film was deposited prior to overgrowth by GaN. The RHEED pattern exhibited a superposition of streaks and V-shaped chevrons indicative of faceting. Indeed, the AFM micrographs of this sample showed the characteristic plateau-valley morphology of GaN films grown with insufficient Ga flux. Compared to films grown under the same conditions as sample 1, films grown under these conditions exhibit narrower asymmetric reflections, indicating a reduction of the edge dislocation density.

X-ray measurements were performed with a Philips X'Pert PRO<sup>TM</sup> four-circle triple-axis diffractometer equipped with a  $\text{CuK}\alpha_1$  source in the focus of a multilayer x-ray mirror and a Ge(022) hybrid monochromator. The detector was kept wide open and at fixed position  $2\theta_B$ , leading to an angular acceptance of  $1^\circ$ . All asymmetric rocking curves were recorded in skew geometry.<sup>5</sup>

We denote the GaN reflections in the form  $hk.l$  which is

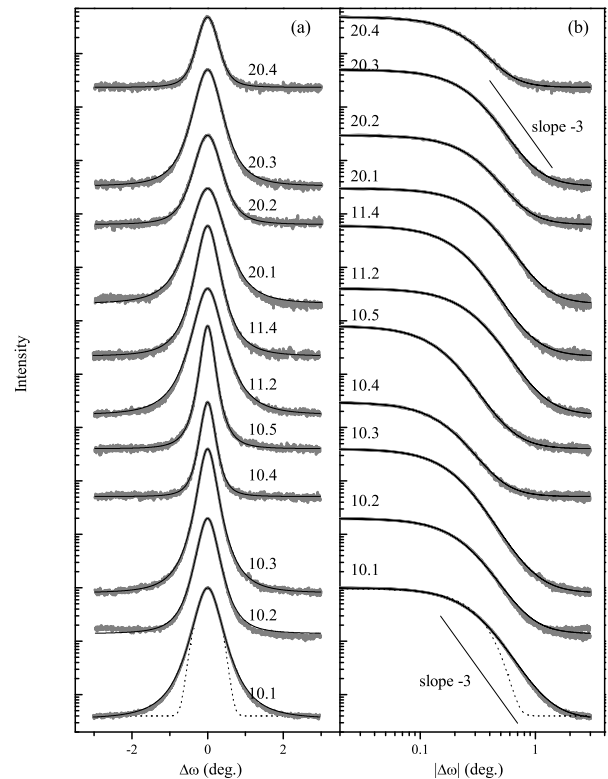


FIG. 4: Double-crystal rocking curves from sample 1 obtained in skew geometry for various different reflections as indicated in the figure. The profiles are shown in logarithmic (a) and log-log (b) scales. The experimental data are shown by gray lines. The full black lines are fits of the intensity by Eq. (10). The dotted lines for the 10.1 profile show a Gaussian profile.

equivalent to the four-index notation  $hkil$  for hexagonal crystals with  $h + k + i = 0$ .

## V. RESULTS

### A. X-ray diffraction

Figure 3 compares a double-crystal rocking curve measured with open detector (acceptance  $1^\circ$ ) and a triple-crystal  $\omega$  scan measured with a three-bounce Ge(022) analyzer across the 10.5 reflection for the same GaN film (sample 1). The comparison with the 004 rocking curve from a perfect Si crystal shows that the GaN peak broadening due to instrumental resolution can be neglected. The log-log plots (right column) show that the tails of the intensity distributions follow the asymptotic laws expected for scattering from dislocations,  $I \propto q^{-3}$  for measurements with the open detector and  $I \propto q^{-4}$  in the case of a collimated diffracted beam. Thus, the comparison of these two profiles shows that they contain the same information about lattice distortions in the film. The rocking

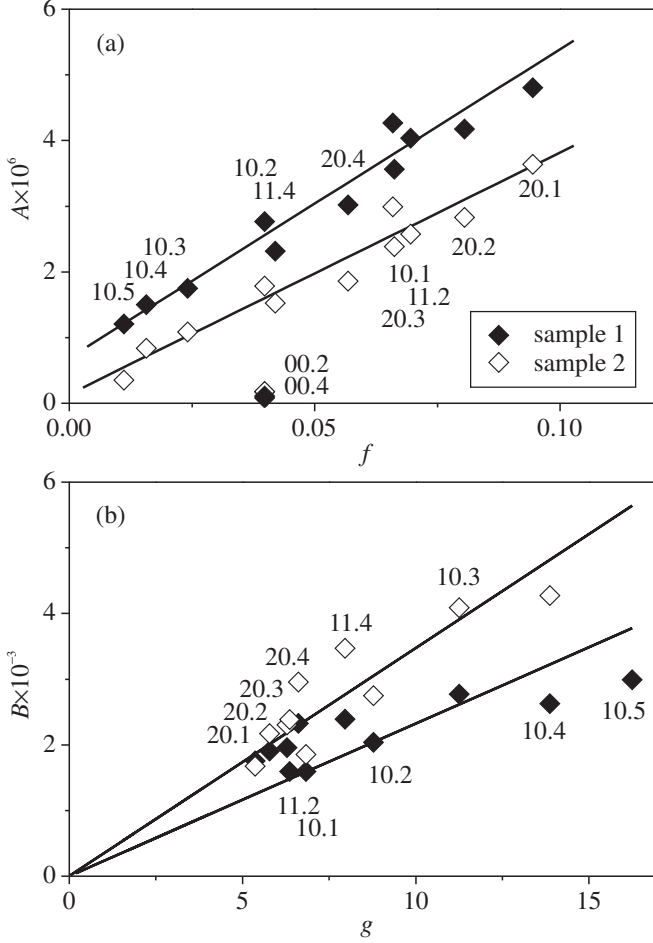


FIG. 5: Parameters  $A$  and  $B$  obtained from the fits of the experimental profiles by Eq. (10). Samples 1 and 2 are denoted by full and open symbols, respectively.

curve measurements with open detector have, however, both experimental and theoretical advantages. The experimental advantage is a two orders of magnitude higher intensity (the intensities are plotted in Fig. 3 in counts per second). The analysis of the rocking curve is also more simple since the intensity distribution is described by the one-dimensional integral (6), while the analysis of the scans with the analyzer requires the two-dimensional integration (5) of the correlation function. Therefore, we restrict ourselves to the analysis of double-crystal rocking curves.

Figure 4 presents skew-geometry rocking curves for various reflections from sample 1. Several conclusions can be drawn just from a direct inspection of the peak profiles. First, the lineshapes are far from being Gaussian at the tails of the intensity distribution: see the comparison of the 10.1 profile with a Gaussian fit [dotted lines in Figs. 4 (a,b)]. When the dynamic range is larger than two orders of magnitude, it is evident that the tails of the asymmetric profiles rather follow the  $q^{-3}$  law. For relatively weak reflections (e. g., 10.4 or 20.4), the  $-3$

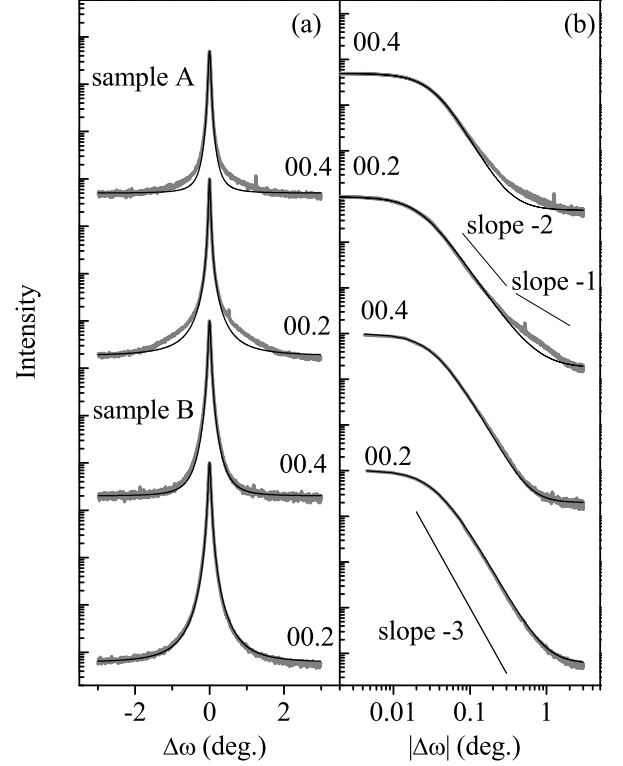


FIG. 6: Symmetric 00.2 and 00.4 x-ray diffraction profiles from samples 1 and 2. The profiles are shown in logarithmic (a) and log-log (b) scales.

exponent is not reached. Thus, the profiles obey the behavior typical for a random dislocation distribution. In the following, we analyze them quantitatively to obtain the characteristics of the dislocation ensemble.

The solid lines in Figs. 4 (a) and (b) are the fits of the measured profiles by Eq. (10). One can see that the peak profiles are adequately described. In Fig. 5, we plot the fit parameters  $A$  and  $B$  as functions of  $f$  and  $g$ , respectively, since according to Eq. (11) both dependencies are expected to be linear. Figure 5 (a) can be considered as a refined version of the Williamson-Hall plot. The linear fit of the data in Fig. 5 for sample 1 crosses the axis of the ordinates at a small but non-zero value of  $A$ , which indicates that, in addition to threading dislocations, there is an additional source of peak broadening, namely, size broadening. This effect is much smaller for sample 2. From the slopes of the straight lines in Fig. 5 (a), we obtain  $\rho_e b_e^2 = A/f = 4.7 \times 10^{-5}$  and  $3.6 \times 10^{-5}$  for samples 1 and 2, respectively, where  $b_e = 0.32$  nm is the length of the Burgers vector of edge dislocations. This result yields a density of edge threading dislocations  $\rho_e = 4.6 \times 10^{10} \text{ cm}^{-2}$  for sample 1 and  $3.5 \times 10^{10} \text{ cm}^{-2}$  for sample 2. The mean distances between edge dislocations are  $r_d = 1/\sqrt{\rho_e} = 47$  nm (sample 1) and 53 nm (sample 2). From the slopes of the lines in Fig. 5 (b), we obtain

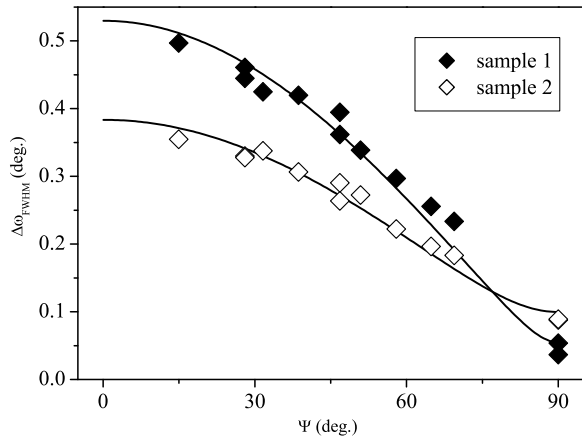


FIG. 7: FWHM of the rocking curves as a function of inclination angle  $\Psi$  for the two GaN films. The symbols are experimental data and the lines are fits to them.

$L/b_e = B/g = 230$  and  $330$ , which give the characteristic lengths of the dislocation correlations  $L = 74$  nm and  $106$  nm, respectively. The dimensionless parameter characterizing the dislocation correlations<sup>28</sup> possesses the values  $M = L/r_d = 1.6$  for sample 1 and  $2.0$  for sample 2.

We also fitted the profiles with Eqs. (14) and (17), which require less computational efforts. These fits give slightly larger values for parameter  $A$  (dislocation density) and are not able to give parameter  $B$  for dislocation correlations.

The symmetric x-ray diffraction profiles shown in Fig. 6 are narrow compared to the asymmetric reflections. Furthermore, the profiles of samples 1 and 2 are qualitatively different. In sample 1, the intensity distributions obey a  $q^{-2}$  law in the intermediate range of angular deviations (and intensities) that is followed by an even lower exponent for large deviations (and very low intensities). In sample 2, the intensity distributions are close to the  $q^{-3}$  law.

Edge threading dislocations with dislocation lines normal to the surface and Burgers vectors in the surface plane, which are the main source of the peak broadening in asymmetric reflections, do not distort the planes parallel to the surface. They do thus not contribute to diffraction in the symmetric reflections. The  $q^{-2}$  law for the 00.2 and 00.4 peaks of sample 1 points to the finite thickness of the epitaxial layer as the main source of the broadening. The  $q^{-1}$  law at the far tails of the peaks are due to another source, possibly thermal diffuse scattering. We did not investigate this part of the symmetric reflections since we suppose that it is not related to threading dislocations which are the topic of the present study. The profiles of sample 2, which is three times thicker than sample 1, obey the  $q^{-3}$  law indicating that the broadening is primarily by dislocations.

The solid lines in Fig. 6 are the fits of the experimental curves to Eq. (20), where the different thicknesses of the layers are explicitly taken into account. We indeed obtain the  $q^{-2}$  intensity decay on the tails of the peak for sample 1 and the  $q^{-3}$  decay for sample 2. From the fit parameters, we obtain  $\rho_s b_s^2 = A/f = 2.4 \times 10^{-6}$  and  $4.5 \times 10^{-6}$  for samples 1 and 2, respectively, where  $b_s = 0.52$  nm is the length of the Burgers vector of screw dislocations. This results yields the screw threading dislocations densities of  $\rho_s = 9 \times 10^8$  cm<sup>-2</sup> for sample 1 and  $1.7 \times 10^9$  cm<sup>-2</sup> for sample 2. From the values of the parameter  $B$  we obtain  $L/b_s = B/g = 650$  and  $440$ , which result in characteristic lengths of the dislocation correlations  $L = 340$  nm and  $230$  nm for sample 1 and 2, respectively. The parameter  $M$  is close to 1 for both samples. Note, however, that screw dislocations are not the only source of the peak broadening in symmetric reflections (see discussion below in Sec. VI).

## B. TEM

TEM is the method of choice to directly determine the character of dislocations and their distribution in thin films. The  $\mathbf{g} \cdot \mathbf{b}$  criterion in TEM is generally applied for the two-beam condition to evaluate the alignment of the strain field of the dislocation with Burgers vector  $\mathbf{b}$  with respect to the diffraction vector  $\mathbf{g}$  producing the image contrast. This criterion is strictly correct for screw dislocations and for edge dislocations only if their line direction  $\mathbf{l}$  and Burgers vector are in the imaging plane, i. e., if  $\mathbf{g} \cdot (\mathbf{b} \times \mathbf{l})$  is considered. In the present case of GaN(0001) films it is well established that three types of threading dislocations exist, having Burgers vectors  $\frac{1}{3}\langle 11\bar{2}0 \rangle$ ,  $\langle 0001 \rangle$  and  $\frac{1}{3}\langle 11\bar{2}3 \rangle$  representing edge, screw and mixed dislocations, respectively, under the assumption that the dislocations lines lie parallel to the  $c$ -axis. Mixed dislocations are not observed in our samples.

In order to identify the Burgers vector, two images have to be recorded with  $\mathbf{g}$  parallel and perpendicular to the  $c$ -axis. The screw dislocations are thus imaged if  $\mathbf{g} = [0002]$ , an example of which is shown in Fig. 8(a) for sample 2. From this image, we can directly measure the dislocation density if we know the TEM specimen thickness that is determined by tilting the interface from the end-on to a well-defined inclined position. Edge dislocations appear in the cross-sectional images if  $\mathbf{g}$  is perpendicular to the  $c$ -axis, e. g., if  $\mathbf{g} = [11\bar{2}0]$ , and we are then able to measure their density in the same way. Furthermore, plan-view TEM imaging is applied to complement the measurement of the dislocation density. Figure 8(b) shows a plan-view TEM image of sample 2, where the specimen is tilted a few degrees off the  $[0001]$  zone axis to obtain two-beam conditions with  $\mathbf{g} = [11\bar{2}0]$  in order to bring the edge dislocations in contrast. The edge threading dislocations are extended along the film normal and homogeneously distributed. It is remarkable that screw dislocations can be identified as well (marked by arrows),



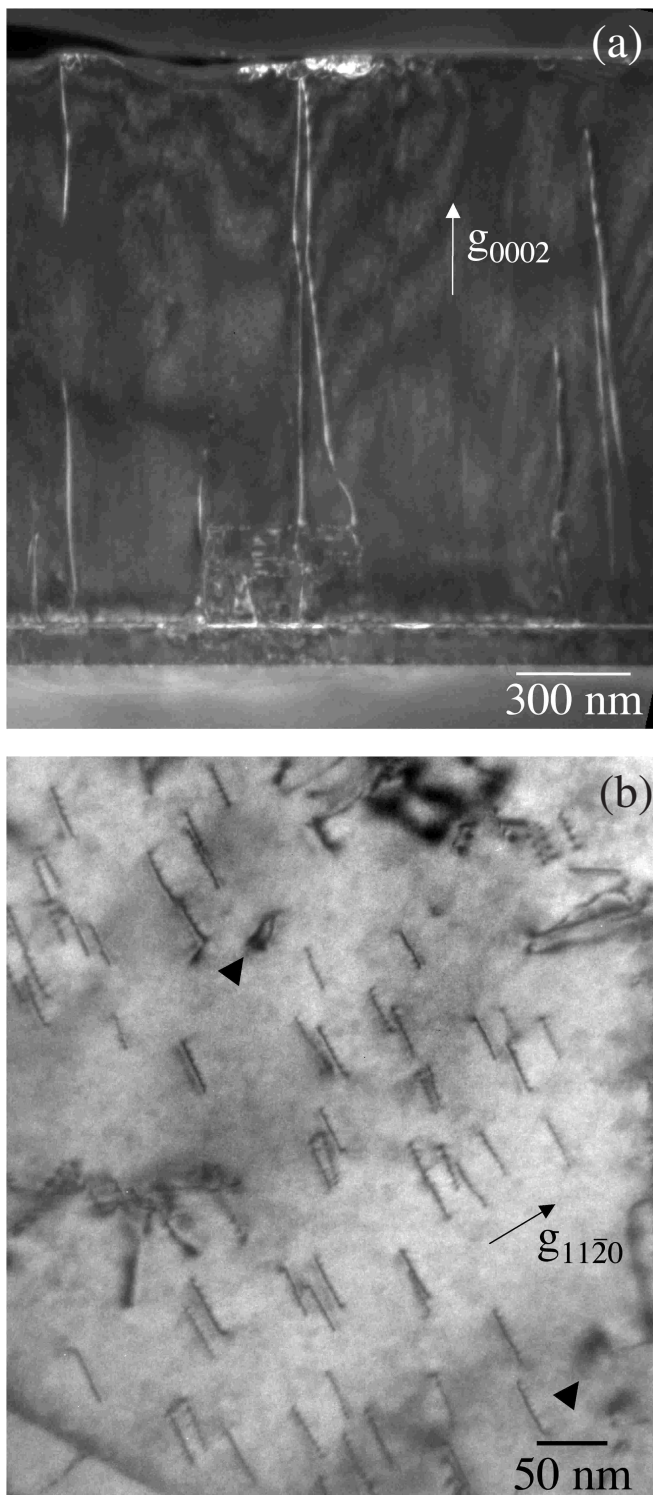


FIG. 8: Cross-sectional (a) and plan-view (b) TEM images of sample 2. The outcrops of screw dislocations are marked in (b) by arrows.

although the contrast should vanish because of  $\mathbf{g} \cdot \mathbf{b} = 0$ . However, this specific contrast is produced due to strain relaxation of the screw dislocation at the free surfaces

TABLE I: Edge and screw dislocation densities determined by x-ray diffraction and TEM.

	thickness (nm)	$\rho_e$ ( $10^{10} \text{ cm}^{-2}$ )		$\rho_s$ ( $10^9 \text{ cm}^{-2}$ )	
		X-ray	TEM	X-ray	TEM
sample 1	340	4.6	$3.0 \pm 0.5$	0.9	—
sample 2	1660	3.5	$2.0 \pm 0.5$	1.7	1.2

varying locally the lattice plane distortions created by the strain field. Table I compares the densities of edge and screw dislocations obtained from the x-ray diffraction and TEM measurements, revealing that the density of edge dislocations is in fact slightly higher in sample 1 compared to sample 2. The screw dislocation density in sample 1 is too low for reliable TEM determination. Some of the screw dislocations are seen as hexagonal pits in AFM micrographs. A lower limit of  $5 \times 10^7 \text{ cm}^{-2}$  is thus obtained for the screw dislocation density in sample 1.

## VI. DISCUSSION

The x-ray diffraction studies of GaN have used, up to now, only the widths of diffraction peaks. Two quantities can be obtained from a series of the reflections.<sup>5</sup> One is the FWHM of the symmetric reflection  $\Delta\omega_s$  which is influenced by screw dislocations but insensitive to edge dislocations. The other quantity is obtained by extrapolation of the FWHM of skew reflections to the limiting case of grazing incidence/grazing exit diffraction, with both incident and diffracted beams lying in the surface plane. This quantity ( $\Delta\omega_e$ ) is sensitive to edge but insensitive to screw dislocations. Figure 7 presents the widths of the diffraction profiles of samples 1 and 2 as a function of the inclination angle  $\Psi$ . The lines are fits by the model described in Ref. 5 to obtain  $\Delta\omega_s$  and  $\Delta\omega_e$ . While these quantities are determined reliably and accurately, the question arises how they are related to the actual dislocation densities. Most commonly,<sup>3,6</sup> the formulas initially proposed in Refs. 40 and 41 for a mosaic crystal are used for this purpose:

$$\rho_e = \frac{\Delta\omega_e^2}{4.35b_e^2}, \quad \rho_s = \frac{\Delta\omega_s^2}{4.35b_s^2}, \quad (21)$$

with the coefficient  $2\pi \ln 2 \approx 4.35$ . In this context, the quantities  $\Delta\omega_s$  and  $\Delta\omega_e$  are often referred to as tilt and twist, respectively.

Equations (21) are valid for mosaic crystals, where the terms tilt and twist describe different modes of relative block misorientation. These terms lose their meaning when applied to a layer with randomly distributed dislocations, since the broadening is then determined by a complicated combination of misorientation of the lattice planes and change of interplanar distances (strain). Hence, equations (21) use an inappropriate approach and

are not strictly valid in the case of a random dislocation distribution. It remains correct that the dislocation density is proportional to the square of the peak width and inversely proportional to the square of the relevant Burgers vector, but the coefficients need to be reconsidered.

The relation between the dislocation density and the FWHM  $\Delta\omega$  of the intensity distribution (10) can be written, by making use of Eqs. (11) and (15), in a form similar to Eq. (21):

$$\rho \approx \frac{\Delta\omega^2}{[2.4 + \ln(g\sqrt{f}M)]^2 fb^2}. \quad (22)$$

The dimensionless parameter  $M = L\sqrt{\rho}$  that characterizes dislocation correlations is slightly larger than 1 for the GaN films studied here, which is an indication of a strong screening of the long-range strain fields of dislocations by the neighboring dislocations. One has  $M \gg 1$  for uncorrelated dislocations. In this latter case, the logarithmic term in Eq. (22) is the one obtained by Krivoglaz.<sup>12,25</sup>

We can now simplify Eq. (22) for the limiting cases of the large-inclination skew diffraction and for symmetric Bragg diffraction by using the expressions for the parameters  $f$  and  $g$  obtained in Sec. III for these cases:

$$\rho_e \approx \frac{4\pi\Delta\omega_e^2 \cos^2 \theta_B}{(3.0 + \ln M)^2 b_e^2}, \quad \rho_s \approx \frac{8\pi\Delta\omega_s^2}{(2.6 + \ln M)^2 b_s^2}. \quad (23)$$

The term  $\ln M$  describing the range of dislocation correlations cannot be neglected even when  $M$  varies between 1 and 2, as it happens to be the case for the samples studied in the present work. Compared to Eqs. (21), Eqs. (23) result in a four times higher edge dislocation density and an order of magnitude higher screw dislocation density and give dislocation densities that are in agreement with the TEM results, see Table I.

There are at least three types of dislocations that may contribute to the broadening of symmetric reflections. First, screw threading dislocations distort the lattice planes parallel to the surface. Secondly, edge threading dislocations can contribute to these reflections if the dislocation lines deviate from the layer normal. Even if such deviations are small, the effect cannot be neglected since the density of edge threading dislocations is much larger than the density of screw threading dislocations. Third, misfit dislocations at the layer-substrate interface contribute to broadening of the symmetric reflections. Although misfit dislocation lines are far from the surface, their non-uniform distortions penetrate through the

whole epitaxial layer.<sup>37</sup> Finally, the stress relaxation at the free surface gives rise to additional strains around the outcrops of the edge threading dislocations, contributing to an additional broadening to the symmetric reflections. Thus, Eq. (10) and, particularly, Eqs. (23) provide an upper estimate of the screw threading dislocation density since they are assumed to be the only source of broadening for symmetric reflections.

## VII. CONCLUSIONS

The width of either symmetric or asymmetric reflection can be used as a figure-of-merit for the dislocation density only if the dislocation distribution is the same in all the samples to be compared. Even for films having a spatially random distribution of dislocations, the width of a given reflection depends not only on the dislocation density, but also on the range of correlations in the restricted random dislocation distribution. The lineshape analysis of the diffraction profile as presented in this work returns the width as well as the correlation range, and is thus a far more reliable approach for estimating the dislocation density than a simple consideration of the width alone.

The lineshape analysis has shown that the x-ray diffraction profiles of the GaN films under investigation are Gaussian only in the central part of the peak. The tails of the peak follow the power laws characteristic to x-ray diffraction of crystals with randomly distributed dislocations. The double-crystal rocking curves measured with a wide open detector follow a  $q^{-3}$  behavior, while the triple-crystal rocking curves with an analyzer crystal obey a  $q^{-4}$  behavior. The study of the double-crystal rocking curves is more simple both experimentally and theoretically, since the diffracted intensity is larger and the peak profile is described by a one-dimensional Fourier transform of the pair correlation function (10).

The  $q^{-3}$  tails of the diffraction profiles are insensitive to correlations between dislocations and allow a more reliable determination of the dislocation densities. The entire diffraction profiles are adequately fitted by Eq. (10). The fits provide two parameters characterizing the dislocation ensemble, the mean dislocation density  $\rho$  and the screening range  $L$ . The latter quantity corresponds to a mean size of the cells with the total Burgers vector equal to zero. We find that, for edge threading dislocations in GaN layers,  $L$  is only slightly larger than the mean distance between dislocations  $\rho^{-1/2}$ .

<sup>1</sup> B. Gil, ed., *Group III Nitride Semiconductor Compounds: Physical and Applications* (Oxford Univ. Press, New York, 1998).

<sup>2</sup> V. Srikant, J. S. Speck, and D. R. Clarke, *J. Appl. Phys.* **82**, 4286 (1997).

<sup>3</sup> T. Metzger, R. Höpler, E. Born, O. Ambacher, M. Stutzmann, R. Stömmer, M. Schuster, H. Göbel, S. Christiansen, M. Albrecht, et al., *Philos. Mag. A* **77**, 1013 (1998).

<sup>4</sup> H. Heinke, V. Kirchner, S. Einfeldt, and D. Hommel, *Appl.*

- Phys. Lett. **77**, 2145 (2000).
- <sup>5</sup> Y. J. Sun, O. Brandt, T. Y. Liu, A. Trampert, and K. H. Ploog, Appl. Phys. Lett. **81**, 4928 (2002).
- <sup>6</sup> R. Chierchia, T. Böttcher, H. Heinke, S. Einfeldt, S. Figge, and D. Hommel, J. Appl. Phys. **93**, 8918 (2003).
- <sup>7</sup> V. Ratnikov, R. Kyutt, T. Shubina, T. Paskova, E. Valcheva, and B. Monemar, J. Appl. Phys. **88**, 6252 (2000).
- <sup>8</sup> A. Munkholm, C. Thompson, C. M. Foster, J. A. Eastman, O. Auciello, P. Fini, S. P. DenBaars, and J. S. Speck, Appl. Phys. Lett. **72**, 2972 (1998).
- <sup>9</sup> C. C. Yang, M. C. Wu, C. H. Lee, and G. C. Chi, J. Appl. Phys. **87**, 2000 (2000).
- <sup>10</sup> W. R. Busing and H. A. Levy, Acta Cryst. **22**, 457 (1967).
- <sup>11</sup> B. E. Warren, *X-Ray Diffraction* (Addison-Wesley, Reading, Mass., 1969).
- <sup>12</sup> M. A. Krivoglaz, *X-Ray and Neutron Diffraction in Non-ideal Crystals* (Springer, Berlin, 1996).
- <sup>13</sup> G. K. Williamson and W. H. Hall, Acta Metall. **1**, 22 (1953).
- <sup>14</sup> M. J. Hordon and B. L. Averbach, Acta Metall. **9**, 237 (1961).
- <sup>15</sup> J. E. Ayers, J. Cryst. Growth **135**, 71 (1994).
- <sup>16</sup> T. Ungár and A. Borbély, Appl. Phys. Lett. **69**, 3173 (1996).
- <sup>17</sup> T. Ungár and G. Tichy, Phys. Stat. Sol. (a) **171**, 425 (1999).
- <sup>18</sup> T. Ungár, J. Gubicza, G. Ribárik, and A. Borbély, J. Appl. Cryst. **34**, 298 (2001).
- <sup>19</sup> B. E. Warren and B. L. Averbach, J. Appl. Phys. **21**, 595 (1950).
- <sup>20</sup> B. E. Warren and B. L. Averbach, J. Appl. Phys. **23**, 497 (1952).
- <sup>21</sup> D. Balzar, J. Appl. Cryst. **25**, 559 (1992).
- <sup>22</sup> D. Balzar and H. Ledbetter, J. Appl. Cryst. **26**, 97 (1993).
- <sup>23</sup> R. A. Young and D. B. Wiles, J. Appl. Cryst. **15**, 430 (1982).
- <sup>24</sup> Th. H. de Keijser, E. J. Mittemeijer, and H. C. F. Rozendaal, J. Appl. Cryst. **16**, 309 (1983).
- <sup>25</sup> M. A. Krivoglaz and K. P. Ryboshapka, Fiz. Met. Metalloved. **15**, 18 (1963), [Phys. Met. Metallogr. **15**, 14 (1963)].
- <sup>26</sup> M. Wilkens, Acta Metall. **17**, 1155 (1969).
- <sup>27</sup> M. Wilkens, *Fundamental Aspects of Dislocation Theory* (Nat. Bur. Stand. (U.S.) Spec. Publ., Washington, D.C., 1970), p. 1195.
- <sup>28</sup> M. Wilkens, Phys. Stat. Sol. (a) **2**, 359 (1970).
- <sup>29</sup> M. A. Krivoglaz, O. V. Martynenko, and K. P. Ryboshapka, Fiz. Met. Metalloved. **55**, 5 (1983).
- <sup>30</sup> J. M. Kosterlitz and D. J. Thouless, J. Phys. C: Solid State Phys. **5**, L124 (1972).
- <sup>31</sup> J. M. Kosterlitz and D. J. Thouless, J. Phys. C: Solid State Phys. **6**, 1181 (1973).
- <sup>32</sup> I. R. Peterson and V. M. Kaganer, Phys. Rev. Lett. **73**, 102 (1994).
- <sup>33</sup> I. Groma, Phys. Rev. B **57**, 7535 (1998).
- <sup>34</sup> M. Wilkens, Phys. Stat. Sol. **3**, 1718 (1963).
- <sup>35</sup> I. Groma, J. Appl. Cryst. **33**, 1329 (2000).
- <sup>36</sup> A. Borbély and I. Groma, Appl. Phys. Lett. **79**, 1772 (2001).
- <sup>37</sup> V. M. Kaganer, R. Köhler, M. Schmidbauer, R. Opitz, and B. Jenichen, Phys. Rev. B **55**, 1793 (1997).
- <sup>38</sup> M. A. Krivoglaz, Fiz. Met. Metalloved. **12**, 465 (1961).
- <sup>39</sup> O. Brandt, R. Muralidharan, P. Waltereit, A. Thamm, A. Trampert, H. von Kiedrowski, and K. H. Ploog, Appl. Phys. Lett. **75**, 4019 (1999).
- <sup>40</sup> P. Gay, P. B. Hirsch, and A. Kelly, Acta Metall. **1**, 315 (1953).
- <sup>41</sup> C. G. Dunn and E. F. Koch, Acta Metall. **5**, 548 (1957).